

Promising Ferroelectricity in 2D Group IV Tellurides: a First-Principles Study

Wenhui Wan,^{*} Chang Liu,^{*} Wende Xiao, and Yugui Yao[†]
*Beijing Key Laboratory of Nanophotonics and Ultrafine Optoelectronic Systems,
 School of Physics, Beijing Institute of Technology, Beijing 100081, China*
 (Dated: December 14, 2024)

Based on the first-principles calculations, we investigated the ferroelectric properties of two-dimensional (2D) Group-IV tellurides XTe (X=Si, Ge and Sn), with a focus on GeTe. 2D Group-IV tellurides energetically prefer a new orthorhombic phase with a highly puckered structure and an in-plane spontaneous polarization. The intrinsic Curie temperature T_c of monolayer GeTe is as high as 290 K and can be further enhanced to 524 K by applying a biaxial tensile strain of 3%. An out-of-plane electric field can effectively decrease the coercive field for the reversal of polarization, extending its potential for regulating the polarization switching kinetics. Moreover, for bilayer GeTe the ferroelectric phase is still the ground state. Combined with these advantages, 2D GeTe is a promising candidate material for practical integrated ferroelectric applications.

PACS numbers: 77.80.-e 77.22.Ej, 77.55.-g

I. INTRODUCTION

Nanoscale devices based on ferroelectric thin films and compatible with Si chips have many potential applications, e.g. ultrafast switching, cheap room-temperature magnetic-field detectors, electrocaloric coolers for computers and nonvolatile random access memories^{1–4}. However, it is still a great challenge to keep the ferroelectricity stable in thin films at room temperature to date⁵. For the conventional ferroelectric materials such as BaTiO₃ or PbTiO₃, the enhanced depolarization field will destroy the ferroelectricity at critical thicknesses of about 12 Å and 24 Å^{6–8}, respectively. To address this challenge, new two-dimensional (2D) ferroelectric phases with ferroelectricity sustained against such a depolarization field are desirable to pave the way for the application of "integrated ferroelectrics".

Compared with their bulk counterparts, 2D materials often lose some symmetry elements (e.g. centrosymmetry) as the result of dimensionality reduction^{9,10}, which favors the appearance of ferroelectricity. A number of 2D ferroelectric phases have been theoretically proposed, e.g. the distorted 1T MoS₂ monolayer¹¹, low-buckled hexagonal IV-III binary monolayers including InP and AsP¹², unzipped graphene oxide monolayer¹³ and monolayer Group-IV monochalcogenides^{14–16}. The Group-IV monochalcogenides including GeS, GeSe, SnS and SnSe have attracted much attention due to their large in-plane spontaneous polarizations \mathbf{P}_s in theory¹⁶ and experimental accessibility. Monolayers of SnSe and GeSe have been successfully synthesized^{17,18}. However, the ground-state SnSe and GeSe multilayers adopt a stacking order that the directions of \mathbf{P}_s in two neighboring layers are opposite¹⁹. Thus, the non-zero polarization only exists in odd-numbered layers, hindering their ferroelectric applications. Excitingly, a robust ferroelectricity has been experimentally observed in SnTe(001) few-layers²⁰. Compared with the low Curie temperature $T_c = 98$ K in bulk SnTe²¹, the T_c in monolayer SnTe was greatly enhanced to 270 K, due to the suppression of the Sn-vacancy and

the in-plane expansion of the lattice^{5,20}. Meanwhile, the \mathbf{P}_s in 2D SnTe are aligned along the in-plane $\langle 110 \rangle$ direction, in contrast to the $\langle 111 \rangle$ direction in bulk²². This behavior again indicates that the dimensionality reduction favors the formation of new ferroelectric phases. However, the ferroelectric properties of 2D SnTe predicted in theory are inconsistent with the experimental measurements²⁰. This calls for a microscopic understanding of the relevant physics. Additionally, the discovery of the ferroelectricity in 2D SnTe shades light on the possible ferroelectric phase in other Group-IV tellurides. Bulk GeTe is ferroelectric and exhibits a rhombohedral crystal structure²³. No crystal phase has been identified in bulk SiTe, but several thermodynamically stable phases of 2D SiTe have been theoretically proposed²⁴. To date, the ferroelectric properties of both 2D GeTe and 2D SiTe remain unexplored.

In this work, we investigated the structural, electronic and ferroelectric properties of 2D Group-IV tellurides XTe (X=Si, Ge and Sn). We found that 2D Group-IV tellurides prefer a new highly puckered structure with an in-plane spontaneous polarization. During the reversal of polarization, monolayer SiTe undergoes a semiconductor-to-metal transition, while monolayer GeTe and SnTe keep semiconducting and ferroelectric. The T_c in monolayer GeTe is as high as 290 K and can be further enhanced to 524 K by applying a biaxial tensile strain of 3%. The in-plane coercive field can be dramatically decreased by a vertical electric field. Moreover, bilayer GeTe exhibits a ferroelectric ground state that the polarization of each layer is aligned parallel. These novel properties provide 2D GeTe a promising material for future nanoscale ferroelectric applications. Finally, we discuss the significant role that the anisotropic tensile strain plays in the room-temperature ferroelectricity of 2D SnTe observed in experiment.

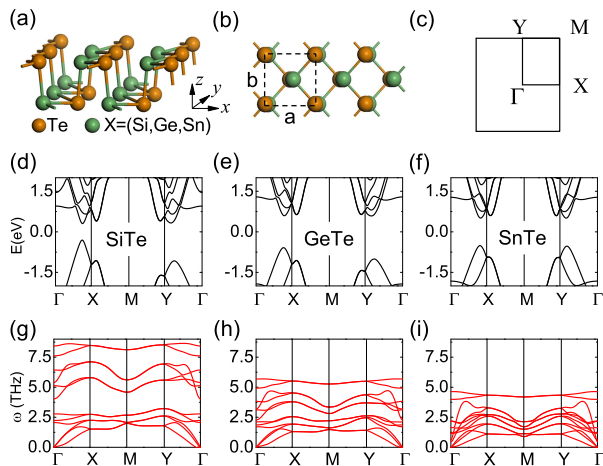


FIG. 1. (a, b) Side and top views of the crystal structure of monolayer XTe (X=Si, Ge and Sn), respectively. (c) 2D first Brillouin zone. (d-f) Band structures of monolayer SiTe, GeTe and SnTe, respectively. (g-i) Phonon dispersions of monolayer SiTe, GeTe and SnTe, respectively.

II. COMPUTATIONAL METHODS

The first-principles calculations were performed using the Vienna ab initio simulation package (VASP)^{25,26} with the projector augmented wave (PAW)²⁷ pseudopotentials and Perdew, Burke, and Ernzerhof (PBE)²⁸ exchange-correlation functionals. The lattice structure and ions positions were fully relaxed until the force on each ion was smaller than 0.005 eV/Å. The OptB86b-vdw functional²⁹ was adopted for the description of Van de Waals interaction in bilayers. The band structures were calculated with Heyd-Scuseria-Ernzerhof (HSE06) hybrid functional³⁰. An energy cut of 450 eV and a $16 \times 16 \times 1$ Monkhorst-Pack³¹ k-point mesh were used. The spontaneous polarization P_s was calculated using the Berry phase approach based on the Kohn-Sham wavefunctions³². The reversal of P_s was simulated by the nudged-elastic-band (NEB) methods³³. The test of spin-orbit coupling (SOC) showed that the relevant ferroelectric physics were marginally affected, thereby we here focus on the results without SOC included. The interaction between nearest neighboring dipole moments in a supercell was described in the mean-field approximation^{15,34}. The Monte Carlo (MC) simulations of the effective Hamiltonian are performed in a supercell of $70 \times 70 \times 1$ unit cells to minimize the size effect. We run 100000 MC sweeps to reach the thermal-equilibrium state, followed by 200000 MC sweeps for the averaging of polarizations and energies. At certain temperature, a number of configurations of supercell with different initial distributions of polarizations are adopted to check the reliability of final averaging.

III. RESULTS AND DISCUSSION

A. Structural, electronic and ferroelectric properties

The total energies of monolayers Group-IV tellurides in different phases were calculated to identify the ground-state crystal structure, which can be seen from the table S1 of supplemental materials (SM)³⁵. Although both bulk GeTe and SnTe exhibit a rhombohedral structure^{21,23}, their monolayers energetically prefer a new orthorhombic phase with a highly puckered structure (see Fig. 1(a)). This novel phase is different from the low-buckled hexagonal phase extracted from the bulk³⁵, in line with previous results³⁶. As displayed in Fig. 1(b), **a** and **b** are the lattice vectors along the *x* (puckered) and *y* (zigzag) directions, respectively. The optimized lattice constants are given in Table I. Each of the four

TABLE I. The lattice constants (*a*, *b*), and band gap E_g of monolayer SiTe, GeTe and SnTe. The lattice constant of monolayer SnTe in theory is inconsistent with the experimental value²⁰ (displayed in brackets). This mismatch might originate from the anisotropic strain that is discussed in the main text.

	<i>a</i> (Å)	<i>b</i> (Å)	E_g (eV)
SiTe	4.294	4.112	0.606
GeTe	4.382	4.242	1.181
SnTe	4.577(4.5811 ²⁰)	4.553 (4.4411 ²⁰)	1.025

atoms in a unit cell is 3-fold coordinated with the atoms of the other species. No imaginary frequency is observed in the phonon dispersions (see Figs. 1(g-i)), confirming their structural stability. The calculated band structures of monolayer Group-IV tellurides are shown in Figs. 1(d-f). The trend of the band gaps is $E_g(\text{GeTe}) > E_g(\text{SnTe}) > E_g(\text{SiTe})$ (see Table I). The anomalous order of E_g might be the result of the fine balance between the relative atomic energy levels and the repulsion between the levels. A similar phenomenon has been reported in lead chalcogenides^{37,38}. The analysis of orbital components of the electron wave function shows that the Te- $p_{(x,y)}$ orbital and the $p_{(x,y)}$ orbital of the Group-IV atom dominate the highest valence band and the lowest conduction band, respectively. The anisotropy of the band structure and phonon dispersion decreases from monolayer SiTe to monolayer SnTe, consistent with the decrease of the anisotropy of their lattice constants (see Table I).

In such an orthorhombic structure, the Group-IV atoms displace along the *x*-direction with respect to the Te atoms, leading to the break of the centrosymmetry but the perseveration of the *yz*-mirror symmetry. Spontaneous polarization is aligned along the *x*-direction and can be labeled as a scalar P_s . Therefore, the thickness of 2D ferroelectric Group-IV tellurides will not be limited by the aforementioned depolarization field vertical to the slab⁶⁻⁸, but a lateral critical size still exists due to the

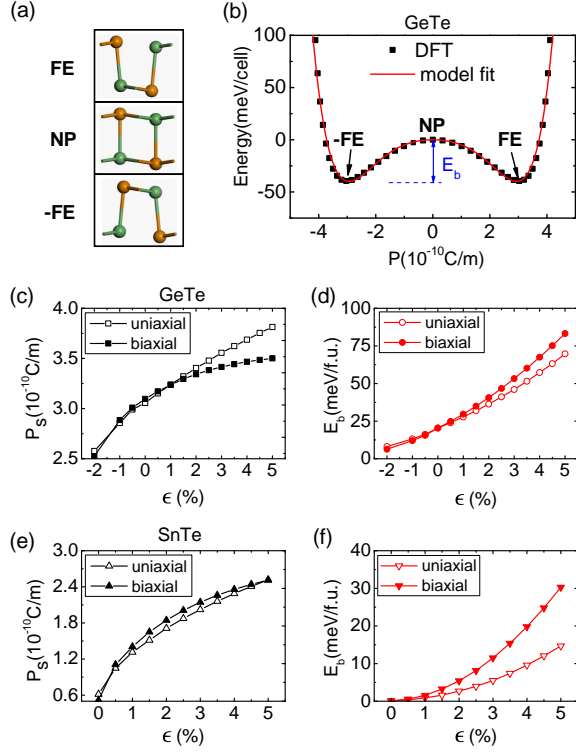


FIG. 2. (a) Two symmetry-equivalent ferroelectric states with opposite in-plane polarizations as well as a high-symmetry, non-polar transition state. (b) Double-well potential of monolayer GeTe vs polarization. E_b is the ferroelectric transition barrier. The red line represents the fitting curve of the Landau-Ginzburg model. The uniaxial and biaxial strains dependence of P_s and E_b for (c, d) monolayer GeTe and (e, f) monolayer SnTe, respectively.

in-plane depolarization field¹⁶. The polarization P_s was calculated by the Berry phase approach³². The reversal of polarization is realized through a phase transition between two symmetry-equivalent ferroelectric states with opposite P_s (labeled as the FE state and -FE state in Fig. 2(a)). By calculating the transition barrier E_b of several pathways using the NEB methods³³, we found that a transition path through a centrosymmetric non-polar (NP) state (see Fig. 2(a)) has the lowest E_b . With this transition path, we calculated the polarization dependence of free energy $F(P)$ and show the result specific to monolayer GeTe in Fig. 2(b). The P_s in the FE state is 3.05×10^{-10} C/m, equivalent to a bulk polarization of $30.5 \mu\text{C}/\text{cm}^2$ if an effective thickness of 1 nm for monolayer GeTe is used. The transition barrier E_b , estimated by the energy difference between the FE and NP states (see Fig. 2(b)), is 20.5 meV per formula unit (f.u.), much smaller than $E_b \approx 200$ meV/f.u. in conventional ferroelectric PbTiO_3 ^{39,40}. This small E_b indicates that the required electric field for the reversal of polarization in monolayer GeTe would be much lower than that in PbTiO_3 .

The ferroelectricity can be substantially affected by the external strain^{41,42}. Here the strain is defined as $\epsilon = (\frac{a}{a_0} - 1) \times 100\%$ where a and a_0 are the lattice constants along the x - or y -direction for the strained and unstrained structures, respectively. The Poisson effect is included in the case of the uniaxial strain. It is found that both uniaxial and biaxial tensile strains ($\epsilon_x = \epsilon_y$) can enlarge the displacement of the Ge atoms with respect to the Te atoms and therefore effectively enhance the P_s and E_b of monolayer GeTe, as shown in Figs. 2(c, d). In contrast, the compressive strain suppresses the P_s and E_b .

Unlike GeTe, the band gap of monolayer SiTe will be closed during the reversal of P_s (see Fig. S2³⁵), leading to a drop of P_s to zero. This semiconductor-metal transition hinders the ferroelectric application of 2D SiTe, but make 2D SiTe suited for the field effect switching devices⁴³.

Monolayer SnTe remains semiconducting during the reversal of P_s . The effective bulk polarization ($P_s = 6.1 \mu\text{C}/\text{cm}^2$) and the transition barrier ($E_b \sim 1$ meV/cell) of monolayer SnTe is very small. After applying a tensile strain, both P_s and E_b can be effectively increased (Figs. 2(e, f)), showing that the ferroelectricity of 2D SnTe can be effectively tuned by strain.

B. Curie temperature

The stability of ferroelectricity is represented by the Curie temperatures T_c at which the macroscopic spontaneous polarization vanishes. Based on the Landau-Ginzburg phase transition theory^{15,44}, the free energy of GeTe supercell is written as a Taylor expansion in terms of the polarization:

$$F = \sum_i \left(\frac{A}{2} P_i^2 + \frac{B}{4} P_i^4 + \frac{C}{6} P_i^6 \right) + \frac{D}{2} \sum_{\langle i,j \rangle} (P_i - P_j)^2, \quad (1)$$

where P_i is the polarization of each unit cell. The first three terms describe the anharmonic double-well potential in a unit cell (see Fig. 2(b)). The last term represents the dipole-dipole interaction between the nearest neighboring unit cells. The parameter D can be estimated by a fitting process in the mean-field approximation¹⁵. All the fitted parameters are given in the table S2³⁵. The Monte Carlo simulations are performed with the effective Hamiltonian of Eq. 1 to investigate the ferroelectric phase transition. As shown in Fig. 3(a), the T_c of unstrained monolayer GeTe is 290 K, near to room temperature. By applying a biaxial strain of 3%, the T_c can be easily enhanced to 524 K, as illustrated in Fig. 3(b).

In contrast, the T_c of unstrained monolayer SnTe is only a few Kelvin (see table S2³⁵). The room-temperature ferroelectricity can be obtained by applying a biaxial strain of 3.5% (see Fig. 3(b)), consistent with aforementioned enhancement of P_s and E_b by tensile strain.

The averaged polarization $\langle P_i \rangle$ in the vicinity of the T_c follows an asymptotic form^{15,45} of $\langle P_i \rangle = C(T_c - T)^\delta$ with $T < T_c$. Here, C is a constant and δ is the critical exponent. For monolayer GeTe, the asymptotic form fits well with the MC simulations, as shown in Fig. 3(a). P_s decreases continuously to zero at T_c . The δ is 0.205, deviating from $\delta=0.5$ in the second-order ferroelectric phase transition⁴⁵. A similar behavior has also been reported in other IV-VI compounds such as SnSe¹⁵, calling for a further study on the type of this phase transition.

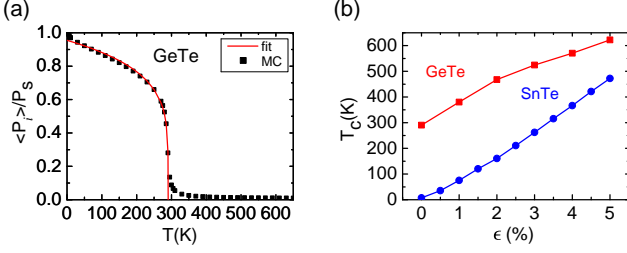


FIG. 3. (a) Temperature dependence of averaged polarization $\langle P_i \rangle$ of monolayer GeTe obtained by the MC simulations. Here the $\langle P_i \rangle$ at different temperature has been normalized with respect to the $\langle P_i \rangle_{T=0K} = P_s$. The red line represents a fitting curve of P_s with an asymptotic form in the vicinity of the Curie temperatures T_c . (b) Biaxial strain dependence of T_c for monolayer GeTe and monolayer SnTe.

C. Coercive field

Based on the Landau-Ginzburg phase transition theory^{44,46}, the electric field \mathcal{E} can be calculated from free energy, i.e. $\mathcal{E} = \frac{\partial F(P)}{\partial P}$. The coercive field \mathcal{E}_c is at the turning points of the hysteresis loop $P(\mathcal{E})$, satisfying the relation of $(\frac{\partial P}{\partial \mathcal{E}})^{-1}|_{\mathcal{E}=\mathcal{E}_c} = 0$. Therefore, the ideal \mathcal{E}_c can be estimated from the maximum slope of the $F(P)$ curve between the NP and FE states¹⁶. A lateral size of $l = 30$ nm is adopted to estimate the effective coercive voltage $V_c = l\mathcal{E}_c$. This lateral size is about the one of latest ferroelectric field effect transistor memory⁴⁷. Through the $F(P)$ curve of monolayer GeTe (Fig. 2(b)), the estimated \mathcal{E}_c is 0.21 V/nm and the effective V_c is 6.3 V. It is noted that the ideal \mathcal{E}_c of the bulk ferroelectric material is always much higher than the experimentally measured \mathcal{E}_c ⁴⁸, due to the formation and movement of the ferroelectric domains. However, the distinction between them at the nanoscale become small as thin ferroelectric films turn out to be more homogeneous than bulk and the formation of ferroelectric domains is suppressed^{45,49}.

It is found that if a vertical electric field \mathcal{E}_\perp was applied, the in-plane displacements of the Ge atoms with respect to the Te atoms will decrease, due to the field-induced coulomb forces. This leads to a reduction of the P_s and E_b (see Fig. 4(a)). As a result, the in-plane coercive field \mathcal{E}_c in monolayer GeTe can be effectively decreased by \mathcal{E}_\perp , as displayed in Fig. 4(b). The maxi-

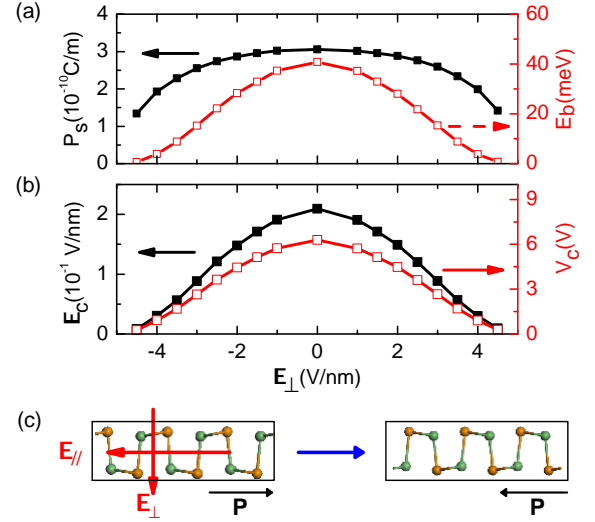


FIG. 4. (a) Vertical electric field \mathcal{E}_\perp dependence of polarization P_s and transition barrier E_b of monolayer GeTe. (b) Vertical electric field \mathcal{E}_\perp dependence of in-plane coercive field \mathcal{E}_c and coercive voltage V_c of monolayer GeTe. (c) A schematic representation of the switching of polarization of monolayer GeTe by a combination of an in-plane electric field \mathcal{E}_\parallel and an out-of-plane electric field \mathcal{E}_\perp .

mum \mathcal{E}_\perp required to tune the \mathcal{E}_c is about 4.5 V/nm (see Fig. 4(b)). The equivalent V_\perp is 4.5 V if an effective thickness of 1 nm for monolayer GeTe is adopted. Fig. 4(c) depicts a feasible way for fast switching the polarization by a combination of two orthogonal electric fields. In this switching process, the required operating voltages are less than 5V, which is desirable for the integration into Si-based semiconducting devices^{2,50}.

D. Bilayer stacking

The stacking order is crucial for the ferroelectricity of multilayers of Group-IV tellurides. We first defined two kinds of stacking order for bilayer GeTe, namely, AA and anti-AA stacking. As shown in Fig. 5, for AA-stacking, the top layer is directly stacked on top of the bottom layer, so that polarization of each layer is aligned parallel. By further shifting the top layer of AA-stacking with $\mathbf{a}/2$, $\mathbf{b}/2$ and $(\mathbf{a} + \mathbf{b})/2$, we can get other three stacking orders labeled as AB, AC and AD stacking. The anti-AA stacking can be gotten if the top layer of the AA-stacked bilayer is rotated around the z axis by 180° . Other stacking orders, e.g. anti-AB, anti-AC and anti-AD can be obtained with a similar process. The energies of bilayer GeTe with different stacking order are shown in table S3³⁵. The bilayer GeTe with the AA stacking has the lowest energy. We note that despite the anti-AA stacking being a meta-stable state, its energy nearly degenerates with that of the AA stacking. Tensile strain can enlarge the energy difference between them. Thus,

the AA stacking becomes the most stable stacking order, as shown in Fig. 5(c).

Assuming that the effective thickness of bilayer is twice of that of monolayer, the effective bulk P_s exhibits a little decrease compared with that of monolayer, due to the fact that the interlayer interaction slightly decrease the in-plane displacement of the Ge atoms with respect to the Te atoms. Tensile strain can also enhance the P_s and E_b of bilayer GeTe with AA stacking (see Fig. 5 (d)). Bilayer SnTe also prefers the AA-stacking but exhibits a weak ferroelectricity. Again, the tensile strain can also enhance its ferroelectric properties. Therefore, 2D GeTe and SnTe take the advantage over aforementioned Group-IV monochalcogenides such as SnSe in ferroelectric application, as the ferroelectricity in 2D SnSe only exist in odd-numbered layers^{15,19}.

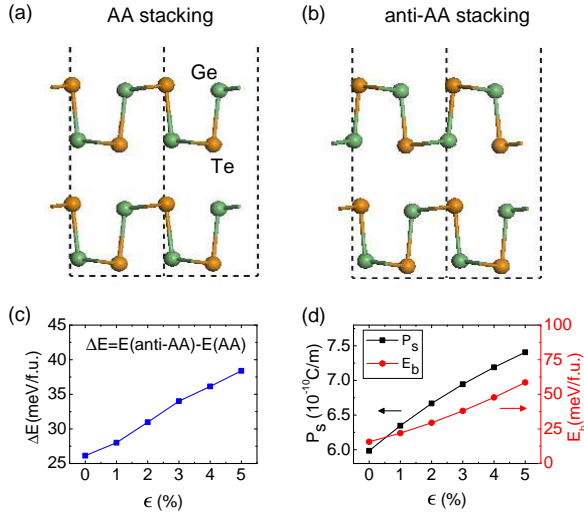


FIG. 5. The (a) AA and (b) anti-AA stacking order for bilayer GeTe. (c) Biaxial strain dependence of energy difference ΔE between bilayer GeTe with the anti-AA stacking and the AA stacking. (d) Biaxial strain dependence of the P_s and E_b of bilayer GeTe with the AA stacking.

E. Discussion

The unique ferroelectricity of 2D GeTe originates from the characters of bonds. When monolayer GeTe is in the NP state (see Fig. 2(a)), the interplay of the ionic and covalent bonding leads to a structural instability⁵, which is represented by the imaginary frequencies in the phonon dispersion, as shown in Fig. S3³⁵. The condensation of these soft modes allows a spontaneous symmetry

breaking and a finite polarization to occur, minimizing the total energy of the system⁵¹. For a comparison, lead chalcogenides have strong ionic bonds and do not exhibit ferroelectricity. For instance, monolayer PbS in the NP state is stable (see Fig. S3³⁵).

It is notable that the predicted ferroelectric properties of strain-free 2D SnTe is inconsistent with the experimental measurements²⁰. We exclude the influence of the computational methods on the prediction. For example, even the relaxed structure of monolayer SnTe using the more advanced Heyd-Scuseria-Ernzerhof (HSE) hybrid functional³⁰ still exhibits a weak ferroelectricity. In the experiments²⁰ the anisotropy between the lattice constant of monolayer SnTe is $(a/b - 1) \times 100\% = 3\%$, while we predicted a small anisotropy of 0.5%. We applied an anisotropic tensile strain of $\epsilon_x = 3.5\%$ and $\epsilon_y = 0.5\%$ to monolayer SnTe and found that the T_c was enhanced from 9 K to 265 K, close to the experimental value of $T_c = 270$ K²⁰. Thus, the observed room-temperature ferroelectricity in 2D SnTe²⁰ might be induced by an anisotropic tensile strain. The external strain can stem from the film-substrate coupling that even exists in the van der Waals epitaxy^{52–54}. Meanwhile, the sensitive response of the ferroelectricity to external strain in 2D SnTe and 2D GeTe also offers a guideline to improve their ferroelectric performance in the future experiments.

IV. CONCLUSION

In summary, we show by the first-principles calculations that 2D GeTe with a highly puckered crystal structure is ferroelectric with an in-plane spontaneous polarization. The Curie temperatures T_c of monolayer GeTe is as high as 290 K. Tensile strain can effectively enhance the T_c and serves as a powerful tool to improve the ferroelectricity of 2D GeTe. The in-plane coercive field for reversing the polarization can be widely tuned by a vertical electric field, facilitating the fast switching of polarization. Furthermore, for bilayer GeTe the ferroelectric phase is still the ground state. With these advantages, 2D GeTe may be the long-sought candidate for realizing the integrated ferroelectric applications.

ACKNOWLEDGMENTS

We acknowledge professor Wei Kang (Peking university) and Dr. Ruixiang Fei (Washington University) for their fruitful discussions. The work is supported by the National Natural Science Foundation of China (Grant No. 11574029) and the MOST Project of China (Nos. 2014CB920903, 2016YFA0300600).

* These two authors contributed equally

† ygyao@bit.edu.cn

- ¹ L. W. Martin and A. M. Rappe, *Nat. Rev. Mater.* **2**, 16087 (2016).
- ² M. Dawber, K. M. Rabe, and J. F. Scott, *Rev. Mod. Phys.* **77**, 1083 (2005).
- ³ J. F. Scott, *Science* **315**, 954 (2007).
- ⁴ A. Lipatov, P. Sharma, A. Gruverman, and A. Sinitskii, *ACS Nano* **9**, 8089 (2015).
- ⁵ B. J. Kooi and B. Noheda, *Science* **353**, 221 (2016).
- ⁶ J. V. Mantese and S. P. Alpay, *Graded ferroelectrics, transcapitors, and transponents* (New York: Springer, 2005).
- ⁷ J. Junquera and P. Ghosez, *Nature* **422**, 506 (2003).
- ⁸ D. D. Fong, G. B. Stephenson, S. K. Streiffer, J. A. Eastman, O. Auciello, P. H. Fuoss, and C. Thompson, *Science* **304**, 1650 (2004).
- ⁹ X. Xu, W. Yao, D. Xiao, and T. F. Heinz, *Nat Phys* **10**, 343 (2014).
- ¹⁰ M. N. Blonsky, H. L. Zhuang, A. K. Singh, and R. G. Hennig, *ACS Nano* **9**, 9885 (2015).
- ¹¹ S. N. Shirodkar and U. V. Waghmare, *Phys. Rev. Lett.* **112**, 157601 (2014).
- ¹² D. Di Sante, A. Stroppa, P. Barone, M.-H. Whangbo, and S. Picozzi, *Phys. Rev. B* **91**, 161401 (2015).
- ¹³ M. Noor-A-Alam and Y.-H. Shin, *Phys. Chem. Chem. Phys.* **18**, 20443 (2016).
- ¹⁴ M. Wu and X. C. Zeng, *Nano Lett.* **16**, 3236 (2016).
- ¹⁵ R. Fei, W. Kang, and L. Yang, *Phys. Rev. Lett.* **117**, 097601 (2016).
- ¹⁶ H. Wang and X. Qian, *2D Materials* **4**, 015042 (2017).
- ¹⁷ L. Li, Z. Chen, Y. Hu, X. Wang, T. Zhang, W. Chen, and Q. Wang, *J. Am. Chem. Soc.* **135**, 1213 (2013).
- ¹⁸ Y. Sun, Z. Sun, S. Gao, H. Cheng, Q. Liu, F. Lei, S. Wei, and Y. Xie, *Adv. Energy Mater.* **4**, 1300611 (2014).
- ¹⁹ L. C. Gomes and A. Carvalho, *Phys. Rev. B* **92**, 085406 (2015).
- ²⁰ K. Chang, J. Liu, H. Lin, N. Wang, K. Zhao, A. Zhang, F. Jin, Y. Zhong, X. Hu, W. Duan, Q. Zhang, L. Fu, Q.-K. Xue, X. Chen, and S.-H. Ji, *Science* **353**, 274 (2016).
- ²¹ M. Iizumi, Y. Hamaguchi, K. F. Komatsubara, and Y. Kato, *J. Phys. Soc. Jpn.* **38**, 443 (1975).
- ²² E. Plekhanov, P. Barone, D. Di Sante, and S. Picozzi, *Phys. Rev. B* **90**, 161108 (2014).
- ²³ D. Di Sante, P. Barone, R. Bertacco, and S. Picozzi, *Advanced Materials* **25**, 509 (2013).
- ²⁴ Y. Chen, Q. Sun, and P. Jena, *J. Mater. Chem. C* **4**, 6353 (2016).
- ²⁵ G. Kresse and J. Hafner, *Phys. Rev. B* **48**, 13115 (1993).
- ²⁶ G. Kresse and J. Furthmüller, *Phys. Rev. B* **54**, 11169 (1996).
- ²⁷ J. P. Perdew, K. Burke, and M. Ernzerhof, *Phys. Rev. Lett.* **77**, 3865 (1996).
- ²⁸ P. E. Blöchl, *Phys. Rev. B* **50**, 17953 (1994).
- ²⁹ J. Klime, D. R. Bowler, and A. Michaelides, *Journal of Physics: Condensed Matter* **22**, 022201 (2010).
- ³⁰ J. Paier, M. Marsman, K. Hummer, G. Kresse, I. C. Gerber, and J. G. ngyn, *J. Chem. Phys.* **124**, 154709 (2006).
- ³¹ H. J. Monkhorst and J. D. Pack, *Phys. Rev. B* **13**, 5188 (1976).
- ³² R. D. King-Smith and D. Vanderbilt, *Phys. Rev. B* **47**, 1651 (1993).
- ³³ G. Henkelman, B. P. Uberuaga, and H. Jansson, *The Journal of Chemical Physics* **113**, 9901 (2000).
- ³⁴ W. Zhong, D. Vanderbilt, and K. M. Rabe, *Phys. Rev. B* **52**, 6301 (1995).
- ³⁵ See Supplemental Material at for the structural and energetical properties of monolayer and bilayer Group IV Tellurides, semiconductor-metal transition in monolayer SiTe, the fitted parameters for the effective Hamiltonian, the energy of bilayer GeTe and SnTe with various stacking orders and the phonon dispersion of non-polar monolayer GeTe and PbS.
- ³⁶ A. K. Singh and R. G. Hennig, *Applied Physics Letters* **105**, 042103 (2014).
- ³⁷ S.-H. Wei and A. Zunger, *Phys. Rev. B* **55**, 13605 (1997).
- ³⁸ U. V. Waghmare, N. A. Spaldin, H. C. Kandpal, and R. Seshadri, *Phys. Rev. B* **67**, 125111 (2003).
- ³⁹ C. Ederer and N. A. Spaldin, *Phys. Rev. B* **74**, 024102 (2006).
- ⁴⁰ R. E. Cohen, *Nature* **358**, 136 (1992).
- ⁴¹ J. H. Haeni, P. Irvin, W. Chang, R. Uecker, P. Reiche, Y. L. Li, S. Choudhury, W. Tian, M. E. Hawley, B. Craigo, A. K. Tagantsev, X. Q. Pan, S. K. Streiffer, L. Q. Chen, S. W. Kirchoefer, J. Levy, and D. G. Schlom, *Nature* **430**, 758 (2004).
- ⁴² W. Siemons, G. J. MacDougall, A. A. Aczel, J. L. Zarestky, M. D. Biegalski, S. Liang, E. Dagotto, S. E. Nagler, and H. M. Christen, *Appl. Phys. Lett.* **101**, 212901 (2012).
- ⁴³ Z. Yang, C. Ko, and S. Ramanathan, *Annu. Rev. Mater. Res.* **41**, 337 (2011).
- ⁴⁴ A. D. Bruce, *Adv. Phys.* **29**, 111 (1980).
- ⁴⁵ V. Fridkin and S. Ducharme, *Ferroelectrics* **466**, 133 (2014).
- ⁴⁶ R. Cowley, *Adv. Phys.* **29**, 1 (1980).
- ⁴⁷ S. Mueller, S. Slesazek, S. Henker, S. Flachowsky, P. Polakowski, J. Paul, E. Smith, J. Miller, and T. Mikolajick, *Ferroelectrics* **497**, 42 (2016).
- ⁴⁸ S. Kim, V. Gopalan, and A. Gruverman, *Appl. Phys. Lett.* **80**, 2740 (2002).
- ⁴⁹ M. J. Highland, T. T. Fister, M.-I. Richard, D. D. Fong, P. H. Fuoss, C. Thompson, J. A. Eastman, S. K. Streiffer, and G. B. Stephenson, *Phys. Rev. Lett.* **105**, 167601 (2010).
- ⁵⁰ I. A. Kornev, H. Fu, and L. Bellaiche, *J. Mater. Sci.* **41**, 137 (2006).
- ⁵¹ U. D. Wdowik, K. Parlinski, S. Rols, and T. Chatterji, *Phys. Rev. B* **89**, 224306 (2014).
- ⁵² H. Cai, E. Soignard, C. Ataca, B. Chen, C. Ko, T. Aoki, A. Pant, X. Meng, S. Yang, J. Grossman, F. D. Ogletree, and S. Tongay, *Adv. Mater.* **28**, 7375 (2016).
- ⁵³ Y. Wang, Y.-Y. Sun, S. Zhang, T.-M. Lu, and J. Shi, *Appl. Phys. Lett.* **108**, 013105 (2016).
- ⁵⁴ K. Zhang, S. Hu, Y. Zhang, T. Zhang, X. Zhou, Y. Sun, T.-X. Li, H. J. Fan, G. Shen, X. Chen, and N. Dai, *ACS Nano* **9**, 2704 (2015), pMID: 25716291.